A Comprehensive Parameterization of Heterogeneous Ice Nucleation of Dust Surrogate: Laboratory Study with Hematite Particles and Its Application to Atmospheric Models

Naruki Hiranuma[a,*], Marco Paukert[a], Isabelle Steinke[a], Kai Zhang[b], Gourihar Kulkarni[b], Corinna Hoose[a], Martin Schnaiter[a], Harald Saathoff[a] and Ottmar Möhler[a]

[a]*Institute for Meteorology and Climate Research – Atmospheric Aerosol Research, Karlsruhe Institute of Technology, Karlsruhe, Germany.*

[b]*Atmospheric Science and Global Change Division, Pacific Northwest National Laboratory, Richland, Washington, USA*

*Corresponding Author. E-mail: seong.moon@kit.edu

Manuscript in preparation for *Atmospheric Chemistry and Physics*

ACP - Special Issue: Results from the ice nucleation research unit (INUIT)

October 1, 2014

Abstract

A new heterogeneous ice nucleation parameterization that covers a wide temperature range (-36 to -78 ˚C) is presented. Developing and testing such an ice nucleation parameterization, which is constrained through identical experimental conditions, is important to accurately simulate the ice nucleation processes in cirrus clouds. The ice nucleation active surface-site density (n_s) of hematite particles, used as a proxy for atmospheric dust particles, were derived from AIDA (Aerosol Interaction and Dynamics in the Atmosphere) cloud chamber measurements under water subsaturated conditions. These conditions were achieved by continuously changing the temperature (T) and relative humidity with respect to ice (RH_{ice}) in the chamber. Our measurements showed several different pathways to nucleate ice depending on T and RH_{ice} conditions. For instance, almost T-independent freezing was observed at -60 ˚C < T < -50 ˚C, where RH_{ice} explicitly controlled ice nucleation efficiency, while both T and RH_{ice} played roles in other two T regimes: -78 ˚C < T < -60 ˚C and -50 ˚C < T < -36 ˚C. More specifically, observations at T lower than -60 ˚C revealed that higher RH_{ice} was necessary to maintain a constant n_s, whereas T may have played a significant role in ice nucleation at T higher than -50 ˚C. We implemented the new hematite-derived n_s parameterization, which agrees well with previous AIDA measurements of desert dust, into two conceptual cloud models to investigate their sensitivity to the new parameterization in comparison to existing ice nucleation schemes for simulating cirrus cloud properties. Our results show that the new AIDA-based parameterization leads to an order of magnitude higher ice crystal concentrations and to an inhibition of homogeneous nucleation in lower temperature regions. Our cloud simulation results suggest that atmospheric dust particles that form ice nuclei at lower temperatures, below -36 ˚C, can potentially have a stronger influence on cloud properties, such as cloud longevity and initiation, compared to previous parameterizations.

1. Introduction

Ice clouds represent a significant source of uncertainty when predicting the Earth's climate change according to the recent Intergovernmental Panel on Climate Change report (i.e., *Chapter 7 of IPCC*, 2013; *Boucher et al*., 2013). Rare airborne particles that can act as ice nucleating particles (INPs) at supercooled temperatures indirectly influence the Earth's forcing by changing microphysical properties of ice clouds, such as reflectivity, longevity and precipitation. However, understanding ice cloud formation over a wide range of atmospherically relevant temperatures and humidity is challenging (e.g., *DeMott et al*., 2011; *Murray et al*., 2012), and our knowledge of ice formation through various nucleation modes is still scarce and limited, such that the ice nucleation processes are currently very poorly represented in global climate models (e.g., *Hoose et al*., 2010; *Liu and Penner*, 2005). In particular, heterogeneous ice nucleation processes proceed through various modes including deposition nucleation, immersion-, condensation- and contact freezing (*Chapter 9 of Pruppacher and Klett*, 1997; *Vali*, 1985). Briefly, deposition mode induces ice formation when water vapor is directly deposited onto the INP, immersion and condensation freezing can induce ice formation when freezing is initiated by the INP immersed within the supercooled droplet or solution droplet, and contact freezing can initiate at the moment when an INP comes into contact with a supercooled droplet.

A global model simulation of INPs in tropospheric clouds showed that more than 85% of heterogeneous ice nucleation results from freezing of supercooled cloud droplets, in which INPs are either immersed or condensed (*Hoose et al*., 2010). However, freezing mechanisms in cirrus clouds are still uncertain (e.g., *Sassen and Khvorostyanov*, 2008). It is understood that various INPs can nucleate ice at water subsaturation and a range of supercooled temperature conditions as comprehensively illustrated in Fig. 2 of *Hoose and Möhler* (2012). The potential importance of ice nucleation under ice supersaturated conditions below the homogeneous freezing threshold line (i.e., Koop line; *Koop et al.*, 2000; *Ren and MacKenzie*, 2005) has already been proved in earlier studies, suggesting the need for further investigations in the water subsaturated region. For example, *Christenson* (2013) experimentally showed that the capillary condensation of supercooled liquid on surface defects facilitated subsequent homogeneous nucleation and growth of ice below water saturation. *Marcolli* (2014) suggested that the inverse Kelvin effect below water saturation helps to form water in pores or cavities and hypothesized that this condensate could freeze through the homogeneous- or immersion mode freezing. This freezing mechanism was referred to as pore condensation and freezing. Previous laboratory studies introduced the concept of a freezing mechanism of solutions on particles at below water saturation (*Zuberi et al*., 2002; *Hung et al*., 2003; *Archuleta et al*., 2005). More recently, *Welti et al*. (2014) explored the relevance of soluble components of mineral dust (i.e., Fluka kaolinite) to condensation freezing below water saturation in the context of classical nucleation theory (CNT). Further, recent aircraft-based field observations suggested that predominant heterogeneous ice formation at cirrus temperatures occurs under water subsaturated conditions, in particular when RH_{ice} is below 140% (*Cziczo et al*., 2013). In addition, *Storelvmo and Herger* (2014) demonstrated that forward modeling simulation with 50% of the mineral dust particles acting as INPs was in good agreement with an observation reported by *Cziczo et al.* (2013). Another airborne observation during an Asian mineral dust event suggested that ice nucleation in cirrus clouds occurs under water subsaturation conditions below 130% RH_{ice} (*Sakai et al*., 2014).

Previously, empirical descriptions given in *Meyers et al*. (1992, hereinafter referred to as M92) were derived from the limited field measurements of ice nuclei concentrations measured at $-23\ ^{\circ}C < T < -7\ ^{\circ}C$ and $102\% < RH_{ice} < 125\%$. Recently, *Phillips et al*. (2008, 2013) empirically parameterized the heterogeneous ice nucleation of various types of aerosols as a function of humidity ($RH_{ice} > 100\%$) and temperature conditions (0 to -100 ˚C). Besides, CNT-based ice nucleation descriptions have also been widely used and implemented in cloud models (e.g., *Barahona and Nenes*, 2009a and 2009b; *Kärcher and Lohmann*, 2003; *Khvorostyanov and Curry*, 2004). These parameterizations can predict different cloud properties for identical environmental conditions. For example, *Barahona et al*. (2010) showed that the ice crystal number can vary by up to an order of magnitude in a global chemical transport model depending on the choice of the heterogeneous ice nucleation parameterization. The authors found the lowest global mean ice crystal concentration from the parameterization of *Phillips et al.* (2008). Moreover, sensitivity of ice cloud properties to the parameterization was observed by *Liu et al*. (2012). They showed that the heterogeneous INP number concentration obtained from a CNT-based parameterization is typically higher by several factors than that of Phillips's parameterization under identical test conditions. To gain insight on what triggers such deviation and to constrain model uncertainties, more and better in situ measurements are necessary (*Cziczo and Froyd*, 2014). In specific, identifying and quantifying sources, global spatio-temporal distribution and mixing-state of INPs might support to reduce model assumptions. In parallel, systematic laboratory measurements are indeed needed to develop water subsaturated ice nucleation parameterizations for the range of atmospherically relevant T-RH_{ice} conditions for a better representation of ice nucleation processes in cloud models and to support in situ measurements.

Recently, *Hoose and Möhler* (2012) compiled previously reported aerosol-specific heterogeneous freezing efficiencies from laboratory experiments based on a single-parameter, n_s (e.g., *Niemand et al*., 2012; *Connolly et al*., 2009). In addition, the authors formulated ice nucleation efficiency by evaluating aerosol-specific "singular" freezing onsets when or after specific ambient conditions were met. Such time-independent and surface area-scaled n_s formulations can be further adapted to comprehensively assess the ice nucleation in a wide range of atmospherically relevant T-RH_{ice} conditions. Accordingly, the n_s concept was adapted to deposition nucleation at low temperatures (up to -80 ˚C).

Within the framework of Ice Nucleation research UnIT (INUIT), we comprehensively investigated the ice nucleation efficiency of pristine cubic hematite particles as a model proxy for atmospheric dust particles. Hematite is used as an example of atmospheric mineral dust particles, which can also be found in the form of cloud-borne particles in shallow stratocumulus clouds (*Matsuki et al*., 2010). Natural hematite often exists in supermicron-sized silt particles and accounts for a few percent of the total dust particle mass (*Claquin et al*., 1999). Ice nucleation efficiencies of cubic hematite particles were measured using the AIDA cloud chamber. We also re-examined the previously reported AIDA results of hematite ice nucleation (*Hiranuma et al*., 2014; *Skrotzki et al*., 2013) and combined them with the results from this work in order to examine the ice nucleation efficiency of hematite particles in the temperature range between -36 and -78 ˚C. In addition to developing the new dust parameterization from these AIDA measurements (Sects. 3.1-3.3), the fitted n_s parameterization was also applied to atmospheric modeling simulations (Sect. 3.4). We implemented the parameterization in the Single column version of the Community Atmospheric Model version 5 (SCAM5, *Neale et al*., 2010) and the COnsortium for Small-scale Modeling (COSMO, *Baldauf et al.*, 2011; *Doms et al.*, 2011) models to assess the newly developed parameterization and compare them with existing parameterizations. It is important to note that the purpose of the current study is to perform a conceptual study with laboratory-synthesized hematite particles as a model aerosol for deposition ice nucleation, over a wide range of T and RH_{ice}, but not to quantify how much hematite content contributes to ice formation in cirrus clouds.

2. Method

2.1. *Description of hematite particles*

Laboratory-generated cubic hematite particles that have homogeneous chemico-physical properties were used as a proxy for atmospheric dust particles. These particles had a uniform composition, morphology and well-defined surface area. Hence, they are suited well for investigating T-RH_{ice}-dependent ice nucleation efficiency and relating it to the surface area (*Hiranuma et al*., 2014). Detailed information on the manufacturing process of cubic hematite particles is available elsewhere (*Sugimoto and Sakata*, 1992). Three different sizes of quasi-monodispersed hematite particles (~200, ~500 and ~1000 nm diameter, respectively) were used in this work. The morphology and size of the hematite particles were characterized by scanning electron microscopy and determined based on an equivalent circle diameter derived from the observed 2D particle projection area (*Vragel*, 2009; *Hiranuma et al*., 2014). A Small-Scale Powder Disperser (SSPD, TSI, Model 3433) was used to dry-disperse the quasi-monodispersed hematite particles into the AIDA vessel as demonstrated in *Skrotzki et al*. (2013).

2.2. *AIDA cooling expansion*

The AIDA expansion freezing experiments were achieved by mechanical pumping (*Möhler et al*., 2003). Mechanical pumps can be operated at different pumping speeds simulating atmospherically relevant adiabatic cooling of rising air parcels in the cylinder of 84 m^3 in volume (i.e., 7 m height x 4 m width thermally conductive aluminum vessel) installed inside the thermostatic housing. For this study, a cooling rate of 5 °C min^{-1} was typically applied at the beginning. Then, the cooling rate decreased to <0.1 °C min^{-1} within 400 s for each pumping expansion experiment, which was mainly due to an increasing heat flux from the chamber walls. Afterwards, an almost constant temperature was maintained by the stirred and well-mixed volume of the cold chamber. During the experiment, the pressure in the vessel decreased from 1000 to 800 mb.

The mean gas temperature in the AIDA vessel was determined by five thermocouples installed at different vertical levels. The sensors of these thermocouples were located about 1 m off the vessel wall and, thus, fully exposed to the chamber air. Stirring of the air by the mechanical ventilator prior to and during pumping ensured a homogeneous temperature distribution in the vessel of ± 0.3 ˚C (*Möhler et al*., 2003). The relative humidities with respect to water (RH_{water}) and RH_{ice} were determined with an accuracy of ± 5% using the mean gas temperature and the mean water vapor concentration. The water vapor concentrations were measured in situ by tunable diode laser (TDL) water vapor absorption spectroscopy throughout the expansion experiments. Since this direct long path absorption technique is described and evaluated in detail in other publications (*Fahey et al*., 2014; *Skrotzki et al*., 2013), no further information is given here.

Under atmospheric pressure, prior to each expansion experiment, a combination of a Scanning Mobility Particle Sizer (SMPS, TSI, Model 3080 DMA and Model 3010 condensation particle counter), an Aerosol Particle Sizer (APS, TSI, Model 3321) and a condensation particle counter (CPC, TSI, Model 3076) collectively measured the total number and size distribution of aerosols at the horizontally extended outlet of the AIDA chamber. Subsequently, the total aerosol surface area was estimated as presented in *Hiranuma et al*. (2014). During expansion, we quantified the ice nucleation of hematite particles with two different light scattering instruments: an optical particle counter welas (PALAS, Sensor series 2300 and 2500) (*Benz* et al., 2005) and SIMONE (German acronym of Streulicht-intensitätsmessungen zum optischen Nachweis von Eispartikeln, which translates to the scattering intensity measurement for the optical detection of ice; *Schnaiter et al*., 2012). More details on the application of this specific combination of two instruments for the AIDA ice nucleation experiments are given in *Hiranuma et al.* (2014).

2.3. Ice nucleation parameterization and modeling

The size-independent singular ice nucleation efficiency, n_s, was calculated by normalizing the observed AIDA ice crystal concentration (N_{ice}) to the total surface area of aerosols, which can be calculated by multiplying the surface area of an individual particle (S_i) by the total number concentration of aerosols (N_{ae}) (e.g., *Niemand et al*., 2012; *Hoose and Möhler*, 2012). For size-selected hematite particles, this linear approximation (i.e., $n_s = (-\ln(1-\alpha))/S_i \sim \alpha/S_i$) was valid independent of the ice active number fraction ($\alpha = N_{ice}/N_{ae}$). An overestimation of ice due to the use of linear approximation only amounted up to about a factor of three at $n_s \leq 10^{12}$

m^{-2}. Subsequently, the n_s values estimated for the wide range of experimental conditions (-36 ˚C < T < -78 ˚C and 100% < RH_{ice} < water saturation) were used to depict and fit constant n_s contour lines. Here, these lines are referred to as the n_s-isolines or simply as the isolines.

The isoline-based parameterizations were derived (see section 3.3) and then implemented in two atmospheric models (a single-column version of a global scale model and a convection resolving model, see Sect 2.3.1. and 2.3.2. for model descriptions). The unique advantages of the use of both models in this study are (1) to demonstrate that our AIDA n_s-based parameterization can be directly applied on different scales of atmospheric models and (2) to estimate the number of ice crystals simulated in two different atmospheric scenarios that complement each other and cover a wide range of atmospheric temperature and saturation conditions (ice formation at higher RH_{ice}, up to ~180%, and lower T, down to ~-70 ˚C). More specifically, the former represents a finely resolved parameterization-oriented model embedded in the global model while the latter is a more physically based high-resolution grid scale model, typically used to analyze small scale complex systems for a fundamental understanding of ice formation. Altogether, results from two independent models were examined for a detailed modeling of atmospheric ice formation on all scales.

The mean size and surface area of hematite particles were prescribed with an assumption that either these particles are spherical and have a mean particle diameter of 1000 nm or the size of these particles follows a lognormal distribution, with a mean volume-equivalent diameter of ~1000 nm (σ_g = 1.05), which is consistent with the AIDA experiments described earlier (*Hiranuma et al*., 2014). The cloud microphysical sensitivity of these two size treatments was characterized. In addition, sensitivity simulations of two lower boundaries of RH_{ice} (i.e., 100 vs. 105%) were also carried out. This sensitivity analysis was specifically useful to examine uncertainty involved in the TDL measurement (RH_{ice} ± 5%) concerning the condensed n_s spacing (up to several orders of magnitude) in a narrow RH_{ice} range and a certain T region. In both models, hematite particle number concentrations are given to be 200 L^{-1}, which is about the average dust concentration simulated by the SCAM5 model over the Southern Great Plain (SGP) site in springtime. Since the n_s-isoline parameterization tested in this study is applicable at T below -36°C, an additional parameterization was used to simulate ice formation of background particles at T > -36°C, namely, the aerosol-independent M92 scheme. These parameterizations were combined to ensure more atmospherically relevant processes and conditions (e.g., distributions of water vapor) when compared to the application of the n_s-isoline parameterization alone.

To better understand to what an extent the AIDA n_s-based parameterization differs from other parameterizations commonly used in atmospheric models, the existing empirical parameterization of heterogeneous ice nucleation by *Phillips et al*. (2013, hereinafter denoted as P13) was implemented as well. The P13 scheme reflects the aerosol specific ice nucleation. In particular, the contribution of mineral dust with the background troposphere baseline surface area mixing ratio of ice-active mineral dust particles (=2.0 x 10^{-6} m^2kg^{-1}) was considered in this study. Ice formation occurring below water saturation only was considered and, thus, Eqn. 1 in *Phillips et al*. (2008) was used for parameterizing ice nucleation.

2.3.1. SCAM5

Single column models are widely used to test physical parameterizations for use in the general circulation model (GCM). The model has 30 vertical levels, and the model time step is set to 10 min. The single column model resembles a single column of a GCM and can be derived from observations or model output. The complex feedbacks between the simulated column and other columns due to large-scale dynamics are not considered. Therefore, the single column model is an ideal tool for testing ice cloud parameterizations. The SCAM5 model was modified to incorporate the new parameterization developed in this study. The *Barahona and Nenes* (2008, 2009a, b) scheme, which provides an analytical solution of the cloud parcel model equations (hereinafter called BN scheme), is used for calculating ice nucleation in cirrus clouds. The new AIDA n_s-isoline-based parameterizations as well as the P13 scheme were implemented in the model. The simulation was performed for one month (April 2010) at the United States Department of Energy's Atmospheric Radiation Measurement facility located at the SGP site (*Hiranuma et al*., 2014).

2.3.2. COSMO

The non-hydrostatic weather forecast model, COSMO, was adapted to systematically investigate the impact of hematite particles under the simulated upper tropospheric conditions.

COSMO is the high-resolution limited-area model to assess clouds and convection at a horizontal spatial resolution of 2.8 km with 50 layers of stretched vertical grids. The time step is set to 20 seconds. In this study, we simulated a period of two days (July 23 to July 25, 2011) on a domain of 450 x 450 horizontal grid points centered over the German Alps (longitude: 0.1°E to 18.7°E, latitude: 41.7°N to 53.2°N). The initial and boundary conditions were provided by the European Centre for Medium-Range Weather Forecasts. They are available at the Meteorological Archival and Retrieval System. In order to account for the spatio-temporal evolution of mass and number densities of six hydrometeor classes (i.e., cloud droplets, raindrops, cloud ice, snow, graupel and hail), the two-moment bulk microphysics scheme was incorporated in our COSMO model version following the method described by *Seifert and Beheng* (2006) and *Seifert et al.* (2012). Apart from the AIDA isoline-based freezing parameterization of hematite, two other ice nucleation modes, namely, M92 and homogeneous nucleation of cloud or solution droplets (*Kärcher et al*., 2006; *Ren and MacKenzie*, 2005), were considered in our COSMO simulations. The latter was used to parameterize the competition of water vapor between homogeneous and heterogeneous freezing.

3. Results

3.1. AIDA ice nucleation experiments

A series of AIDA experiments was carried out during the INUIT01 and INUIT04 campaigns to investigate the ice nucleation efficiency of well-characterized hematite particles under water subsaturated conditions at -47 ˚C < T. In addition, we used the AIDA results reported by *Skrotzki et al*. (2013) and reconciled them with the n_s values in order to parameterize the overall ice nucleation efficiency of hematite particles up to -78 ˚C. In total, 12 expansion experiments, 4 from the INUIT campaigns and 8 from *Skrotzki et al*. (2013), were studied. Detailed experimental conditions and aerosol properties for these expansion experiments are summarized in Table 1. The use of different sizes of hematite particles in different temperature regions was justified by calculating the size-independent n_s values of 200 and 1000 nm diameter particles at ~-40 ˚C. For instance, the evaluated n_s values (10^{10} m^{-2}) for these two sizes agreed very well within ± 1 % RH_{ice} and ± 0.3 ˚C of chamber conditions (see corresponding RH_{ice} and T at Evaluated n_s in Table 1 for INUIT04_08, 1000 nm, HALO06_19, 200 nm, and HALO06_20, 200 nm). This agreement verified the reproducibility of the AIDA chamber experiments, ice nucleation efficiency of hematite particles and size-independence of the n_s calculations. The advantage of using 1000 nm diameter hematite particles was that, due to their comparatively larger surface area, they were efficient in forming ice in cooling expansion experiments at -40 ˚C < T < -36 ˚C (*Hiranuma et al*., 2014).

The temporal profiles of deposition nucleation experiments from HALO campaigns, including N_{ice}, gas T, RH_{ice} and RH_{water} measured by the TDL as well as the polarized light scattering properties in near-backscattering direction measured by SIMONE, are shown in Figure 1. The depolarization ratio, which is sensitive to ice particle nucleation and growth, can be deduced from the latter. During a typical expansion, the air mass in the vessel experiences continuous cooling (for up to 500 s) and an increase in relative humidity (for up to 200 s, Fig. 1 panel i and ii). Figure 1 panel iii shows the temporal plot of the depolarization ratio. At the beginning of the expansion, the depolarization ratio increases because ice is nucleating on the hematite particles. Conversely, repartitioning of gas phase water to ice phase water due to growing ice crystals triggers the declines in both depolarization ratio (i.e., sizing effect, *Schnaiter et al*., 2012) and RH, usually after 100 s. The time-delay in our welas ice detection (typically 1 μm is the minimum ice detection diameter for 200 and 500 nm diameter hematite particles) due to slower depositional growth after ice nucleation at lower T is accounted for in our error analyses (Figure 2). We evaluated only up to several hundred seconds of each expansion experiment as the ice nucleating period. Similar experimental profiles for INUIT campaigns are presented in Figure S1.

The initial n_s-isoline curves in the T-RH_{ice} space are illustrated in Figure 2. Constant n_s-isoline curves are obtained by fitting second degree polynomial fit equations to the constant n_s magnitudes calculated at various T and RH_{ice} (see the supplement for more details). Previous AIDA results of two immersion freezing experiments (i.e., INUIT04_13 and INUIT01_28 from *Hiranuma et al*., 2014) are also shown on the water saturation line and used to constrain the fitted curves because immersion freezing is considered part of isolines. Since the n_s values presented in Fig. 3 of *Hiranuma et al*. (2014) only extends up to ~10^9 m^{-2}, the data points of higher n_s values were extrapolated based on the observed values from two measurements. Figure 2 shows several important features of n_s-isoline curves. First, below −60 ˚C, n_s-isolines showed an increase in RH_{ice} required to maintain a constant n_s (i.e., $n_s > 2.5\times10^8$ m^{-2}) with decreasing T (i.e., RH_{ice}-dependent ice nucleation regime). For example, at a RH_{ice} = 120% and T = -75 ˚C, cooling by 1 ˚C corresponds to a 10% decrease in n_s. This observation is interesting because the increase in RH_{ice} required to maintain constant n_s values is consistent with the CNT for deposition nucleation (Eqn. A11 in *Hoose and Möhler*, 2012). Second, the highest sensitivity of RH_{ice} is observed in a region where n_s-isolines are perpendicular to temperature-isolines (~-60 ˚C < T < ~-50 ˚C). Here, n_s is almost independent of T, and solely dependent on RH_{ice}. Finally, we observed strong T-dependent nucleation near water saturation (i.e., while cooling along the water saturation line towards ~-50 ˚C). At a constant RH_{ice} (e.g., 114%), for example, cooling by 1 ˚C from -41 to -42 ˚C corresponds to an increase in n_s of approximately half an order of magnitude (see inset of Fig. 2). This suggests that the n_s values depend on temperature. Interestingly, we observed a continuous increase in n_s during cooling even after the depletion of supersaturation below -40 ˚C (Figure S2). CNT does not explain this predominant T contribution near water saturation (Fig. A1 in *Hoose and Möhler*, 2012). Therefore, other microphysical processes at the particle surface and/or perhaps even within the bulk phase may be responsible for this T-dependent behavior and these results appear to support the existence of a pore or surface freezing process, as discussed in recent literature (e.g., *Marcolli*, 2014). In particular, we suspect that water condensation on the particle surface plays an important role on subsequent freezing. To support this, the surfaces of our hematite particles are not perfectly smooth and contain some active sites (e.g., pores and steps, *Hiranuma* et al., 2014). Moreover, water vapor may preferably fill the surface cavities due to the reduced saturation pressure in pores or at steps because of negative curvature Kelvin effects (*Marcolli*, 2014), thus leading to namely "surface condensation freezing (SCF)". As described in previously published literatures (*Christenson*, 2013; *Marcolli*, 2014), SCF may be of relevance to homogeneous nucleation (i.e., spontaneous ice nucleation in supercooled aerosol) at relevant T (< -36 ˚C) and/or immersion mode freezing under water subsaturated conditions. Thus, SCF may arise from both homogeneous and heterogeneous nucleation.

3.2. Comparison with previous studies

The n_s-isolines of hematite particles were compared to previous measurements made using different aerosol species. This comparison was performed to (1) confirm that our n_s fit reproduces the overall trend shown by previous studies under certain T-RH$_{ice}$ conditions and (2) to demonstrate that the parameterization with laboratory-synthesized hematite particles quantitatively represents ice nucleation properties of atmospheric dust particles.

Comparison of the hematite n_s-isolines to previous deposition freezing observations are shown in Figure 3. More specifically, previous measurements were performed with natural Saharan desert dust (SD2, *Möhler et al*., 2006), reference Arizona test dust (ATD, *Möhler et al*., 2006; *Welti et al*., 2009), volcanic ash (*Steinke et al*., 2011), soot (*Möhler et al*., 2005), clay minerals (*Welti et al*., 2009; *Koehler et al*., 2010) and organics (*Shilling et al*., 2006; *Wang and Knopf*, 2011). These previous experimental studies used various types of ice nucleation instruments, such as substrate-supported cold stages coupled with an optical microscope (*Shilling et al*., 2006; *Wang and Knopf*, 2011), portable ice nuclei counters (*Koehler et al*., 2010; *Welti et al*., 2009) and the AIDA cloud simulation chamber (*Möhler et al*., 2005; *Möhler et al*., 2006; *Steinke et al*., 2011). They revealed the importance of both RH$_{ice}$ and temperature onto deposition mode ice nucleation of specific particle compositions. In Fig. 3a, previous AIDA results for dusts, ash and soot, are presented. Specifically, we utilized the T-RH$_{ice}$ data at α =

0.08 of SD2 and ATD reported in the previous AIDA study (*Möhler et al*., 2006) to define isolines. It is noteworthy that an α of 0.08 corresponds to ~ 10^{11} m^{-2} in n_s when assuming uniform distributions of spherical particles of 0.5 μm diameter ($n_s = (-\ln(1-\alpha))/(\pi(0.5\text{x}10^{-6})^2)$), which is in good agreement with the 10^{11} m^{-2} n_s-isoline of hematite particles. For volcanic ash, we adapted n_s values (10^9, 5 x 10^9 and 10^{10} m^{-2}) originally reported in *Steinke et al*., (2011). *Möhler et al*. (2005) found that the ice nucleation of soot starts at the initial increase in polarized light scattering intensity in near-backscattering direction at 488 nm (n_s values are inaccessible). Except for these AIDA studies, other isolines in Fig. 3b and c were defined based on the reported ice nucleation measurements. For instance, *Koehler et al.* (2010) studied the deposition mode nucleation of size-selected (i.e., 200 nm, 300 nm, 400 nm) natural dusts, and reported ice nucleation conditions (T and RH_{ice}) of ATD at α = 0.01 and of Canary Island Dust and Saharan Dust at α = 0.05. *Welti et al*. (2009) also studied the deposition nucleation abilities of size-segregated mineral dusts (i.e., 100 to 800 nm diameter of ATD, illite, kaolinite and montmorillonite) based on α = 0.01. *Shilling et al.* (2006) reported the ice nucleation onsets of ammonium sulfate and maleic acid detected by the decreasing partial pressure of water with FTIR-reflection absorption spectroscopy (e.g., 1 in 10^5 nucleation at about -33 ˚C for a spherical particle size of 1 to 10 μm diameter). *Wang and Knopf.* (2011) investigated deposition freezing of various mineral and organic particles including kaolinite, Suwannee River standard fulvic acid and Leonardite standard humic acid particles. The authors reported the mean size of particles and associated ice-activated fractions at the given T-RH_{ice}.

As seen in Fig. 3, the results from previous studies suggest the necessity of increasing RH_{ice} to maintain a constant n_s value below T ~-55°C. They also indicate that nucleation may be triggered by SCF in the region where data and isolines approach water saturation where temperature plays a significant role on ice nucleation. It can also be observed that the contour of our new n_s-isoline parameterization of cubic hematite particles in T-RH_{ice} coordinates generally agrees with the onsets determined by previous studies of other atmospherically relevant aerosols. In particular, the n_s-isolines estimated from ATD and SD2 (~10^{11} m^{-2}, Fig. 3a), which reasonably agree with the hematite n_s-isoline, suggest that atmospheric dust may have similar deposition mode ice nucleation efficiency.

3.3. n_s-isoline-based parameterizations

Next, the ice nucleation efficiency of hematite particles was parameterized over a wide range of T-RH_{ice}. Three types of parametrical descriptions used in this study are shown in Figure 4. First, based on the AIDA experimental results, a series of constant n_s curves was interpolated to produce isolines in the range of 10^6 m^{-2} < n_s < 10^{12} m^{-2} (Fig. 4a). The lower bound of n_s value (10^6 m^{-2}) was set based on the minimum n_s observed during AIDA expansions. Since the certain regions of n_s-isolines (i.e., n_s < 7.5 x10^{10} m^{-2}; blue lines in Fig. 2) can submerge below ice saturation, the correction was applied to shift them and maintain all isolines above 100% RH_{ice}. The procedure to constrain n_s to >100% RH_{ice} is described in the supplement (Fig. S3). Above the upper bound of 10^{12} m^{-2}, n_s presumably remains constant up to the water saturation line in the T -RH_{ice} space (no experimental data is available in this range). This assumption is valid in the present study because this n_s upper limit was hardly reached in our modeling case. However, more cloud simulation chamber measurements and data points for n_s >> 10^{12} m^{-2} are required to correctly constrain the n_s upper limit. It also has to be noted that the modeled ice crystal number concentration (L^{-1}) derived from ice nucleation of hematite in this study is approximated by multiplying n_s by a simulated total surface of hematite (6.3 x 10^{-10} m^2 L^{-1}).

In the second fit approach (Fig. 4b), the interpolated n_s values were used to formulate the n_s-isoline with a third degree-polynomial fit as a function of T (˚C) and RH_{ice} (%) as

$$n_s^{3d}(T, \mathrm{RH_{ice}}) = -3.777 \times 10^{13} - 7.818 \times 10^{11} \cdot T + 4.252 \times 10^{11} \cdot \mathrm{RH_{ice}} - 4.598 \times 10^{9} \cdot T^2 + 6.952 \times 10^{9} \cdot T \cdot \mathrm{RH_{ice}} - 1.111 \times 10^{9} \cdot \mathrm{RH_{ice}}^2 - 2.966 \times 10^{6} \cdot T^3 + 2.135 \times 10^{7} \cdot T^2 \cdot \mathrm{RH_{ice}} - 1.729 \times 10^{7} \cdot T \cdot \mathrm{RH_{ice}}^2 - 9.438 \times 10^{5} \cdot \mathrm{RH_{ice}}^3$$

for -78 ˚C < T < -36 ˚C and 100 % < RH_{ice} < water saturation (1)

where $n_s^{3d}(T, RH_{ice})$ is the n_s derived from the third degree fit. The resulting spatial plot of isolines for constant n_s is shown in Fig. 4b. Note that the upper temperature boundary of −36 ˚C was assigned as the interface between immersion mode- and deposition mode ice nucleation (*Hiranuma et al*., 2014), and the lower boundary of −78 ˚C is the limit introduced by interpolating the hematite-isoline curves. The third approach (Fig. 4c) consisted in applying the equivalent n_s for deposition nucleation of hematite particles parameterized using the method introduced by *Phillips et al*. (2008 and 2013). In detail, we characterized the nucleation activity solely of mineral dust through the deposition mode by adapting the Equation (1) from *Phillips et al*. (2008), which accounts for nucleation under water subsaturated conditions, and excluded the contribution at water saturation, i.e., Equation (2) of *Phillips et al*. (2008). AIDA n_s-isoline-based parameterization suggests strong supersaturation dependence of n_s at low T. Observed diversity between a new parameterization (Figs. 4a and 4b) and P13 (Fig. 4c) may result in different ice crystal forming propensities and may predict different cloud properties. The potential consequence of observed diversity is demonstrated using conceptual models and discussed in the following section.

3.4. Model simulations

The SCAM5 results for monthly mean profiles of the simulated in-cloud N_{ice} ($Ni \sim N_{ice}$) over the ARM SGP site for five cases are shown in Figure 5. These include (Case 1) the pure homogeneous ice nucleation case, (Case 2-4) cases with contributions from both homogeneous and heterogeneous ice nucleation (hereinafter referred to as the combined case) described in Fig. 4a-c (corresponding to Simulations A, B and C) and (Case 5) the simulation of the different lower boundaries of RH_{ice} (RH_i^*, Simulation D). In addition, the observed profile of ice crystal number concentrations is also shown in comparison to the simulations in Fig. 5. The observational data were collected over the SGP site on eight days of April 2010 during the Small PARTicles In CirrUS (SPARTICUS) campaign (*Zhang et al*., 2013). The results of our simulations suggests that ice crystal formation due to heterogeneous ice nucleation processes inhibits homogeneous ice nucleation and significantly reduces the ice number concentrations for the AIDA parameterizations (Fig. 4a and b). In contrast, due to the much smaller ice crystal production from P13, as shown by the pure heterogeneous case in Figure 5, homogeneous ice nucleation in the P13 case (Fig. 4c) is less affected by heterogeneous nucleation. The observed mean profile of in-cloud ice crystal number concentrations is in agreement with the simulated ones. The differences between the three parameterizations derived from AIDA measurements, corresponding to Simulations A, B and D, are small for both the combined case and the pure heterogeneous ice nucleation case as presented in Fig. 6. This is because the BN scheme used in SCAM5 is based on parcel model theory and uses the predicted maximum ice supersaturation (S_{max}) to calculate deposition ice nucleation rates. S_{max} is determined by assuming that the supersaturation will reach its maximum where the depletion of water vapor compensates the supersaturation increase from cooling in a cloud parcel (i.e., BN scheme). The three parameterizations (i.e., Simulations A, B and D) have largest differences when RH_{ice} is below 120% while S_{max} calculated in the model is often larger than 115%. This also explains the low sensitivity of N_{ice} to the lower bound of the onset RH_{ice} value (Figs. 5 and 6). We also investigated the impact of different particle size distributions on the calculation (not shown). The impact is small and negligible. The negligible sensitivity to the choice of AIDA parameterizations in SCAM5 simulations (Simulation A and B of Figs. 5 and 6) as well as the negligible sensitivity to the lower bound of the RH_{ice} value for ice nucleation, RH_i^* in Figs. 5 and 6, reflect the limitation of SCAM5 as a large-scale model, which can't explicitly resolve the sub-grid (for the GCM grid box) variability of the supersaturation.

The results of the COSMO model for the vertical profiles of N_{ice} (presumably equivalent to the heterogeneous INP number concentration) are summarized in Figure 7. These results simulate the three different parameterization schemes (corresponding to Fig. 4a-c) in combination with homogeneous freezing. N_{ice} was spatially averaged over all areas of the model domain which in principle allow for deposition nucleation in our simulations, i.e. conditions below -36°C and above 100% RH_{ice}. Because not always n_s is larger than zero (white areas of Fig. 2), also areas without ice formation are contained. It is also noteworthy that only purely heterogeneous ice formation is presented rather than the total ice occurring in the model. As shown in Fig. 7, the mean N_{ice} resulting from the parameterization based on P13 is smaller than that obtained from the AIDA n_s-isoline-based parameterization by more than two orders of magnitude. This large difference results predominantly from the inactivity of P13 at low RH_{ice}. Unlike the SCAM5 results, the COSMO results show the sensitivity to the different lower boundaries of RH_{ice} (i.e., RH_i^* = 105%, Simulation D). For instance, the mean N_{ice} below -36 ˚C with a higher RH_{ice} boundary (105%) is reduced by 12%. This difference is perhaps due to the use of finely resolved grid-scale humidity in COSMO rather than parameterizing S_{max} as done in SCAM5 (*Gettelman et al.*, 2010). Figure 8 illustrates the differences between P13 and the AIDA results depending on T and RH_{ice}. Simulated N_{ice} values are segregated in fine T and RH_{ice} spacing (1K and 2% bins, respectively) based on the thermodynamic conditions under which ice crystals were formed in COSMO and summed up over the time of simulation. This segregation allows for an estimation of the relative contribution of different thermodynamic conditions to the simulated ice formation. Our results show diversity between P13 and the AIDA n_s-isoline-based parameterization. Ice crystal formation was less for P13 and more for the new parameterization. A possible explanation for the observed deviation may be due to the difference in parameterization based on lab- or field data. For instance, atmospheric aging and processing (i.e., surface coating and associated heterogeneous surface reactions) may have altered ice-nucleating propensity and limited deposition nucleation of dust-derived INPs in the P13 parameterization for the field data-derived parameterization as discussed in *Phillips et al*. (2008).

4. Discussions

As described in the previous section (Sect. 3.1), deposition mode freezing cannot solely explain the n_s-isoline observation below water saturation (-50 ˚C < T < -36 ˚C in Fig. 2). Although we presumed that SCF acts as a subset of immersion freezing and plays an important role in this region, further insight and evidence of SCF beyond cloud simulation chamber observations are required to correctly understand the contributions of both homogeneous and heterogeneous nucleation. High-resolution microscopic techniques with an integrated continuous cooling setup are needed to visualize the freezing process of a single particle and to fully understand the complex freezing processes involved in SCF on particle surfaces.

Comparison of the new parameterization to a previous empirical parameterization (P13) showed that the new AIDA n_s-isoline-based scheme predicts more ice (Figs. 4-8). In particular, T-RH_{ice} dependence of N_{ice} and n_s at low T that may coincide in the upper troposphere, and this highlights the need for further investigations. However, it should be noted that there is some evidence for the atmospheric relevance and applicability of the new parameterization. First of all we demonstrated that the new n_s parameterization based on the experiments with hematite particles agrees well with previous literature results for mineral dust aerosol (e.g., *Möhler et al,* 2006; *Welti et al*., 2009; *Köhler et al*., 2010). Second, *Niemand et al*. (2012) demonstrated that different dusts exhibit similar n_s in immersion mode freezing and perhaps such a similarity remains true for the deposition mode ice nucleation of desert dusts. Lastly, the comparison between the observed profile of ice crystal number concentrations and the simulated ones (Figs. 5 and 6) also suggests the validity of the new parameterization. These premises must be further examined in comparing to atmospherically relevant substrates (fresh and aged ones) and their ice nucleation activities in laboratory settings. In situ INP measurements, such as the number concentration and the types of INPs, at the upper troposphere can also help to constrain the parameterization.

Finally, to further develop more atmospherically relevant parameterizations other than the fit-based parameterization with artificial test aerosol, the relationship between $1/T$ and $\ln S_{ice}$ for a constant nucleation rate or n_s based on the CNT can be analyzed (i.e., Eqns. A10-A11 in *Hoose and Möhler*, 2012). In this way, the composition specific $n_s(T\text{-}S_{ice})$ values, where the transition from SCF to deposition nucleation (or vice versa) occurs, may be better defined and can be then be used as an inexpensive model friendly parameterization.

5. Conclusion

A new heterogeneous ice nucleation parameterization was developed using results obtained from AIDA cloud simulation chamber experiments. The new n_s-isoline-based parameterization is applicable to a wide temperature range from -36 to -78 ˚C and, hence, allows for the examination of ice nucleation spectra in a simple framework for modeling application.

Our experimental results provide a good basis for the T and RH_{ice} dependence of deposition nucleation, and the formulated hematite n_s-isolines are comparable to that of desert dust samples. Consequently, our results with synthesized hematite particles can also be relevant to cirrus applications despite their smaller atmospheric relevance compared to natural hematite. Our isoline formulation suggested three different ice nucleation pathways over the wide range of temperature. In specific, a RH_{ice}-dependent ice nucleation regime was observed at temperatures below ~-60 ˚C, where deposition mode is presumably responsible to trigger ice nucleation. At -60 ˚C < T < -50 ˚C, ice nucleation efficiency was T-independent (i.e., RH_{ice} dependent). Conversely, a predominant influence of T on ice nucleation was observed near the water saturation condition (T > ~-50 ˚C), which may be indicative of nucleation due to condensation of water at the particle surface followed by homogeneous freezing of the condensed water (i.e., SCF). The observed active SCF near water saturation and physical processes at the transitions of nucleation modes still remain to be studied in detail for various types of atmospheric particles.

Our conceptual model examinations also considered the competition between heterogeneous freezing and homogeneous freezing of solution particles to evaluate the relative importance of the different freezing processes in two models (SCAM5 and COSMO). The inhibition of homogeneous nucleation due to heterogeneous freezing was commonly observed in both SCAM5 and COSMO simulations. Our new parameterization revealed a minimum deviation of N_{ice} values estimated by SCAM5 at minimum RH_{ice} values for ice formation (100 or 105%) compared to COSMO. This deviation suggests different sensitivities of the model to the lower bound of the RH_{ice} value owing to the presence of the model-resolved supersaturation to calculate the ice nucleation rate. Overall, our new hematite-based parameterization strongly suggests the role of T and more ice nucleation when compared to the existing empirical parameterization, presumably allowing more ice activation under water subsaturated conditions.

Author Contributions

N. Hiranuma and O. Möhler designed and conceived the experiments. Parameterizations were implemented by N. Hiranuma, I. Steinke and M. Paukert. M. Paukert and K. Zhang carried out modeling studies with input from C. Hoose, N. Hiranuma and G. Kulkarni. M. Schnaiter analyzed SIMONE data. H. Saathiff contributed to TDL measurements and analysis. The manuscript was written by N. Hiranuma. All authors discussed the results and contributed ideas to the manuscript.

Acknowledgements

This work was supported by the German Research Foundation (Deutsche Forschungsgemeinschaft, DfG) under contracts MO 668/4-1 and HO 4612/1-1 within the Research Unit FOR 1525 (INUIT) and by the Helmholtz Association's research programme "Atmosphere and Climate (ATMO)". The authors acknowledge partial financial support by DfG and Open Access Publishing Fund of Karlsruhe Institute of Technology. K. Zhang and G. Kulkarni acknowledge support from the Department of Energy Atmospheric System Research Program. The Pacific Northwest National Laboratory is operated for DOE by Battelle Memorial Institute under contract DE-AC05-76RLO 1830. We would like to thank R. Buschbacher, T. Chudy, E. Kranz, G. Scheurig and S. Vogt for their professional support for the AIDA chamber operation during the INUIT campaigns. We also thank P. Weidler and S. Jaeger for support in preparing the hematite particles. M. Hummel's contribution to the model setup is gratefully acknowledged.

References

Archuleta, C. M., DeMott, P. J., and Kreidenweis, S. M.: Ice nucleation by surrogates for atmospheric mineral dust and mineral dust/sulfate particles at cirrus temperatures, Atmos. Chem. Phys., 5, 2617−2634, doi:10.5194/acp-5-2617-2005, 2005.

Baldauf, M., Seifert, A., Förstner, J., Majewski, D., Raschendorfer, M., and Reinhardt, T.: Operational convective-scale numerical weather prediction with the COSMO model: Description and sensitivities, Mon. Weather Rev., 139, 12, 3887–3905, doi: 10.1175/MWR-D-10-05013.1, 2011.

Barahona,,D. and Nenes, A.: Parameterization of cirrus cloud formation in large-scale models: Homogeneous nucleation, J. Geophys. Res., 113, D11211, doi:10.1029/2007JD009355, 2008.

Barahona, D. and Nenes, A.: Parameterizing the competition between homogeneous and heterogeneous freezing in cirrus cloud formation – monodisperse ice nuclei, Atmos. Chem. Phys., 9, 369–381, doi:10.5194/acp-9-369-2009, 2009a.

Barahona, D. and Nenes, A.: Parameterizing the competition between homogeneous and heterogeneous freezing in ice cloud formation – polydisperse ice nuclei, Atmos. Chem. Phys., 9, 5933–5948, doi:10.5194/acp-9-5933-2009, 2009b.

Barahona, D., Rodriguez, J., and Nenes, A.: Sensitivity of the global distribution of cirrus ice crystal concentration to heterogeneous freezing, J. Geophys. Res., 115, D23213, doi:10.1029/2010JD014273, 2010.

Benz, S., Megahed, K., Möhler, O., Saathoff, H., Wagner, R., and Schurath, U.: *T*-dependent rate measurements of homogeneous ice nucleation in cloud droplets using a large atmospheric simulation chamber, J. Photoch. Photobio. A, 176, 208–217, doi:10.1016/j.jphotochem.2005.08.026, 2005.

Boucher, O., Randall, D., Artaxo, P., Bretherton, C., Feingold, G., Forster, P., Kerminen, V.-M., Kondo, Y., Liao, H., Lohmann, U., Rasch, P., Satheesh, S. K., Sherwood, S., Stevens, B., and Zhang, X. Y.: Clouds and Aerosols. In: Climate Change 2013: The Physical Science Basis. Contribution of Working Group I to the Fifth Assessment Report of the Intergovernmental Panel on Climate Change [Stocker, T. F., D. Qin, G.-K. Plattner, M. Tignor, S. K. Allen, J. Boschung, A. Nauels, Y. Xia, V. Bex, and P. M. Midgley (eds.)]. Cambridge University Press, Cambridge, United Kingdom and New York, NY, USA, 2013.

Christenson, H.: Two-step crystal nucleation via capillary condensation, Cryst. Eng. Comm., 15, 2030–2039, doi:10.1039/C3CE26887J, 2013.

Claquin, T., Schulz, M., and Balkanski, Y.: Modeling the mineralogy of atmospheric dust sources, J. Geophys. Res., 104, 22243–22256, doi:10.1029/1999JD900416, 1999.

Connolly, P.J., Möhler, O., Field, P.R., Saathoff, H., Burgess, R., Choularton, T., and Gallagher, M.: Studies of heterogeneous freezing by three different desert dust samples, Atmos. Chem. Phys., 9, 2805–2824, doi:10.5194/acp-9-2805-2009, 2009.

Cziczo, D. J., Froyd, K. D., Hoose, C., Jensen, E. J., Diao, M., Zondlo, M. A., Smith J. B., Twohy, C. H., and Murphy, D. M.: Clarifying the dominant sources and mechanisms of cirrus cloud formation, Science, 340, 1320–1324, doi:10.1126/science.1234145, 2013.

Cziczo, D. J. and Froyd, K. D.: Sampling the composition of cirrus ice residuals, Atmospheric Research, 142, 15−31, doi: 10.1016/j.atmosres.2013.06.012, 2014.

DeMott, P. J., Möhler, O., Stetzer, O., Vali, G., Levin, Z., Petters, M. D., Murakami, M., Leisner, T., Bundke, U., Klein, H., Kanji, Z. A., Cotton, R., Jones, H., Benz, S., Brinkmann, M., Rzesanke, D., Saathoff, H., Nicolet, M., Saito, A., Nillius, B., Bingemer, H., Abbatt, J., Ardon, K., Ganor, E., Georgakopoulos, D. G., and Saunders, C.: Resurgence in ice nuclei measurement research, Bulletin of the Amer. Meterol. Soc, 92, 1623–1625, doi:http://dx.doi.org/10.1175/2011BAMS3119.1, 2011.

Doms, G., Förster, J., Heise, E., Herzog, H.-J., Mironov, D., Raschendorfer, M., Reinhardt, T., Ritter, B., Schrodin, R., Schulz, J.-P., and Vogel, G.: A description of the nonhydrostatic regional COSMO Model. Part II: Physical parameterization, Technical Report. Deutscher Wetterdienst, 154 pp, 2011.

Fahey, D. W., Gao, R.-S., Möhler, O., Saathoff, H., Schiller, C., Ebert, V., Krämer, M., Peter, T., Amarouche, N., Avallone, L. M., Bauer, R., Bozóki, Z., Christensen, L. E., Davis, S. M., Durry, G., Dyroff, C., Herman, R. L., Hunsmann, S., Khaykin, S. M., Mackrodt, P., Meyer, J., Smith, J. B., Spelten, N., Troy, R. F., Vömel, H., Wagner, S., and Wienhold, F. G.: The AquaVIT-1 intercomparison of atmospheric water vapor measurement techniques, Atmos. Meas. Tech. Discuss., 7, 3159–3251, doi:10.5194/amtd-7-3159-2014, 2014.

Gettelman, A., Hegglin, M. I., Son, S.-W., Kim, J., Fujiwara, M., Birner, T., Kremser, S., Rex, M., Añel, J. A., Akiyoshi, H., Austin, J., Bekki, S., Braesike, P., Brühl, C., Butchart, N., Chipperfield, M., Dameris, M., Dhomse, S., Garny, H., Hardiman, S. C., Jöckel, P., Kinnison, D. E., Lamarque, J. F., Mancini, E., Marchand, M., Michou, M., Morgenstern, O., Pawson, S., Pitari, G., Plummer, D., Pyle, J.A., Rozanov, E., Scinocca, J., Shepherd, T. G., Shibata, K., Smale, D., Teyssèdre, H., and Tian, W.: Multimodel assessment of the upper troposphere and lower stratosphere: Tropics and global trends, J. Geophys. Res., 115, D00M08, doi:10.1029/2009JD013638, 2010.

Hiranuma, N., Hoffmann, N., Kiselev, A., Dreyer, A., Zhang, K., Kulkarni, G., Koop, T., and Möhler, O.: Influence of surface morphology on the immersion mode ice nucleation efficiency of hematite particles, Atmos. Chem. Phys., 14, 2315–2324, doi:10.5194/acp-14-2315-2014, 2014.

Hoose, C., Kristjánsson, J.E., Chen, J.-P., and Hazra, A.: A classical-theory-based parameterization of heterogeneous ice nucleation by mineral dust, soot and biological particles in a global climate model, J. Atmos. Sci., 67(8) 2483–2503, doi:http://dx.doi.org/10.1175/2010JAS3425.1, 2010.

Hoose, C and Möhler, O.: Heterogeneous ice nucleation on atmospheric aerosols: a review of results from laboratory experiments, Atmos. Chem. Phys., 12, 9817–9854, doi:10.5194/acp-12-9817-2012, 2012.

Hung H.-M., Malinowski, A., and Martin, S. T.: Kinetics of heterogeneous ice nucleation on the surfaces of mineral dust cores inserted into aqueous ammonium sulfate particles, J. Phys. Chem. A., 107, 1296–1306, doi: 10.1021/jp021593y, 2003.

Kärcher, B. and Lohmann, U.: A parameterization of cirrus cloud formation: Heterogeneous freezing, J. Geophys. Res., 108, 4402, doi:10.1029/2002JD003220, 2003.

Kärcher, B., Hendricks, J., and Lohmann, U.: Physically based parameterization of cirrus cloud formation for use in global atmospheric models, J. Geophys. Res., 111, D01, 205, doi:10.1029/2005JD006219, 2006.

Khvorostyanov, V. I. and Curry, J. A.: The theory of ice nucleation by heterogeneous freezing of deliquescent mixed CCN. Part I: Critical radius, energy, and nucleation rate, J. Atmos. Sci., 61, 2676–2691, doi:http://dx.doi.org/10.1175/JAS3266.1, 2004.

Koehler, K. A., Kreidenweis, S. M., DeMott, P. J., Petters, M. D., Prenni, A. J., and Möhler, O.: Laboratory investigations of the impact of mineral dust aerosol on cold cloud formation, Atmos. Chem. Phys., 10, 11955–11968, doi:10.5194/acp-10-11955-2010, 2010.

Koop, T., Luo, B., Tsias, A., and Peter, T.: Water activity as the determinant for homogeneous ice nucleation in aqueous solutions, Nature, 406, 611–614, doi:10.1038/35020537, 2000.

Liu, X. and Penner, J. E.: Ice nucleation parameterization for global models, Meteorol. Z., 14, 499–514, doi:10.1127/0941-2948/2005/0059, 2005.

Liu, X., Shi, X., Zhang, K., Jensen, E. J., Gettelman, A., Barahona, D., Nenes, A., and Lawson, P.: Sensitivity studies of dust ice nuclei effect on cirrus clouds with the Community Atmosphere Model CAM5, Atmos. Chem. Phys., 12, 12061–12079, doi:10.5194/acp-12-12061-2012, 2012.

Marcolli, C.: Deposition nucleation viewed as homogeneous or immersion freezing in pores and cavities, Atmos. Chem. Phys., 14, 2071–2104, doi:10.5194/acp-14-2071-2014, 2014.

Matsuki, A., Schwarzenboeck, A., Venzac, H., Laj, P., Crumeyrolle, S., and Gomes, L.: Cloud processing of mineral dust: direct comparison of cloud residual and clear sky particles during AMMA aircraft campaign in summer 2006, Atmos. Chem. Phys., 10, 1057–1069, doi:10.5194/acp-10-1057-2010, 2010.

Meyers, M. P., DeMott, P. J., and Cotton, W. R.: New primary ice nucleation parameterizations in an explicit cloud model, J. Appl. Meteorol., 31, 708–721, doi:http://dx.doi.org/10.1175/1520-0450(1992)031<0708:NPINPI>2.0.CO;2, 1992.

Möhler, O., Stetzer, O., Schaefers, S., Linke, C., Schnaiter, M., Tiede, R., Saathoff, H., Krämer, M., Mangold, A., Budz, P., Zink, P., Schreiner, J., Mauersberger, K., Haag, W., Kärcher, B., and Schurath, U.: Experimental investigation of homogeneous freezing of sulphuric acid particles in the aerosol chamber AIDA, Atmos. Chem. Phys., 3, 211–223, doi:10.5194/acp-3-211-2003, 2003.

Möhler, O., Linke, C., Saathoff, H., Schnaiter, M.,Wagner, R., Mangold, A., Krämer, M., and Schurath, U.: Ice nucleation on flame soot aerosol of different organic carbon content, Meteorol. Z., 14, 477–484, doi:10.1127/0941-2948/2005/0055, 2005.

Möhler, O., Field, P. R., Connolly, P., Benz, S., Saathoff, H., Schnaiter, M., Wagner, R., Cotton, R., Krämer, M., Mangold, A., and Heymsfield, A. J.: Efficiency of the deposition mode ice nucleation on mineral dust particles, Atmos. Chem. Phys., 6, 3007–3021, doi:10.5194/acp-6-3007-2006, 2006.

Murray, B. J., O'Sullivan, D., Atkinson, J. D., and Webb, M. E.: Ice nucleation by particles immersed in supercooled cloud droplets, Chem. Soc. Rev., 41, 6519–6554, doi:10.1039/c2cs35200a, 2012.

Neale, R. B., Chen, C-.C., Gettelman , A., Lauritzen, P. H., Park, S., Williamson, D. L., Conley, A. J., Garcia, R., Kinnison, D., Lamarque, J-.F., Marsh, D., Mills, M., Smith, A. K., Tilmes, S., Vitt, F., Morrison, H., Cameron-Smith, P., Collins, W. D., Iacono, M. J., Easter, R. C., Ghan, S. J., Liu, X., Rasch, P. J., and Taylor, M. A.: Description of the NCAR Community At- mosphere Model (CAM5.0), Tech. Rep. NCAR/TN-486-STR, NCAR, available at: http://www.cesm.ucar.edu/models/cesm1.0/cam/ (last access: 8 January 2013), 2010.

Niemand, M., Möhler, O., Vogel, B., Vogel, H., Hoose, C., Connolly, P., Klein, H., Bingemer, H., DeMott, P., Skrotzki, J., and Leisner, T.: A particle-surface-area-based parameterization of immersion freezing on mineral dust particles, J. Atmos. Sci., 69, 3077–3092, doi:http://dx.doi.org/10.1175/JAS-D-11-0249.1, 2012.

Phillips, V. T. J., DeMott, P. J., and Andronache, C.: An empirical parameterization of heterogeneous ice nucleation for multiple chemical species of aerosol, J. Atmos. Sci., 65, 2757–2783, doi:http://dx.doi.org/10.1175/2007JAS2546.1, 2008.

Phillips, V. T. J., DeMott, P. J., Andronache, C., Pratt, K. A., Prather, K. A., Subramanian, R., and Twohy, C.: Improvements to an empirical parameterization of heterogeneous ice nucleation and its comparison with observations, J. Atmos. Sci., 70, 378–409, doi: http://dx.doi.org/10.1175/JAS-D-12-080.1, 2013.

Pruppacher, H. R. and Klett, J. D.: Microphysics of Clouds and Precipitation, Atmospheric and Oceanographic Sciences Library, Kluwer Academic Publishers, Dordrecht, The Netherlands, 309–360, 1997.

Ren, C. and Mackenzie, A. R.: Cirrus parameterization and the role of ice nuclei, Q. J. Roy. Meteorol. Soc., 131, 1585–1605, doi:10.1256/qj.04.126, 2005.

Sakai, T., Orikasa, N., Nagai, T., Murakami, M., Tajiri, T., Saito, A., Yamashita, K., and Hashimoto, A.: Balloon-borne and Raman lidar observations of Asian dust and cirrus cloud properties over Tsukuba, Japan, J. Geophys. Res., 119, 3295–3308, doi:10.1002/2013JD020987, 2014.

Sassen, K. and Khvorostyanov, V. I.: Cloud effects from boreal forest fire smoke: Evidence for ice nucleation from polarization lidar data and cloud model simulations, Environ. Res. Lett., 3, 025006, doi:10.1088/1748-9326/3/2/025006, 2008.

Schnaiter, M., Büttner, S., Möhler, O., Skrotzki, J., Vragel, M., and Wagner, R.: Influence of particle size and shape on the backscattering linear depolarisation ratio of small ice crystals – cloud chamber measurements in the context of contrail and cirrus microphysics, Atmos. Chem. Phys., 12, 10465–10484, doi:10.5194/acp-12-10465-2012, 2012.

Seifert, A. and Beheng, K. D.: A two-moment cloud microphysics parameterization for mixed-phase clouds. Part I: Model description, Meteorol. Atmos. Phys., 92, 45–66, doi:10.1007/s00703-005-0112-4, 2006.

Seifert, A., Köhler, C., and Beheng, K. D.: Aerosol-cloud-precipitation effects over Germany as simulated by a convective-scale numerical weather prediction model, Atmos. Chem. Phys., 12 (2), 709–725, doi:10.5194/acp-12-709-2012, 2012.

Shilling, J. E., Fortin, T. J., and Tolbert, M. A.: Depositional ice nucleation on crystalline organic and inorganic solids, J. Geophys. Res., 111, D05207, doi:10.1029/2005JD006664, 2006.

Skrotzki, J., Connolly, P., Schnaiter, M., Saathoff, H., Möhler, O., Wagner, R., Niemand, M., Ebert, V., and Leisner, T.: The accommodation coefficient of water molecules on ice – cirrus cloud studies at the AIDA simulation chamber, Atmos. Chem. Phys., 13, 4451–4466, doi:10.5194/acp-13-4451-2013, 2013.

Steinke, I., Möhler, O., Kiselev, A., Niemand, M., Saathoff, H., Schnaiter, M., Skrotzki, J., Hoose, C., and Leisner, T.: Ice nucleation properties of fine ash particles from the Eyjafjallajökull eruption in April 2010, Atmos. Chem. Phys., 11, 12945–12958, doi:10.5194/acp-11-12945-2011, 2011.

Storelvmo, T. and Herger, N.: Cirrus cloud susceptibility to the injection of ice nuclei in the upper troposphere, J. Geophys. Res., 119, 2375–2389, doi:10.1002/2013JD020816, 2014.

Sugimoto, T. and Sakata, K.: Preparation of monodisperse pseudocubic α-Fe_2O_3 particles from condensed ferric hydroxide gel, J. Colloid Interface Sci., 152, 2, 587–590, doi:10.1016/0021-9797(92)90062-Q, 1992.

Vali, G.: Nucleation terminology, J. Aerosol Sci., 16, 575–576, doi:10.1016/0021-8502(85)90009-6, 1985.

Vragel, M.: Messung klimarelevanter optischer Eigenschaften von Mineralstaub im Labor, Faculty of Physics, Karlsruhe Institute of Technology, Karlsruhe, 162 pp., 2009.

Wang, B. and Knopf, D.: Heterogeneous ice nucleation on particles composed of humic-like substances impacted by O_3, J. Geophys. Res., 116, D03205, doi:10.1029/2010JD014964, 2011.

Welti, A., Lüönd, F., Stetzer, O., and Lohmann, U.: Influence of particle size on the ice nucleating ability of mineral dusts, Atmos. Chem. Phys., 9, 6705–6715, doi:10.5194/acp-9-6705-2009, 2009.

Welti, A., Kanji, Z. A., Lüönd, F., Stetzer, O., and Lohmann, U.: Exploring the mechanisms of ice nucleation on kaolinite: from deposition nucleation to condensation freezing, J. Atmos. Sci., 71, 16–36, doi: 10.1175/JAS-D-12-0252.1, 2014.

Zhang, K., Liu, X., Wang, M., Comstock, J. M., Mitchell, D. L., Mishra, S., and Mace, G. G.: Evaluating and constraining ice cloud parameterizations in CAM5 using aircraft measurements from the SPARTICUS campaign, Atmos. Chem. Phys., 13, 4963-4982, doi:10.5194/acp-13-4963-2013, 2013.

Zuberi, B., Bertram, A. K., Cassa, C. A., Molina, L. T., and Molina, M. J.: Heterogeneous nucleation of ice in (NH4)2SO4−H2O particles with mineral dust immersions, Geophys. Res. Lett., 29, 1504, doi:10.1029/2001GL014289, 2002.

Table and Figures of "A Comprehensive Parameterization of Heterogeneous Ice Nucleation of Dust Surrogate: Laboratory study with Hematite Particles and Its Application to Atmospheric Models"

October 1, 2014

Naruki Hiranuma[a,*], Marco Paukert[a], Isabelle Steinke[a], Kai Zhang[b], Gourihar Kulkarni[b], Corinna Hoose[a], Martin Schnaiter[a], Harald Saathoff[a] and Ottmar Möhler[a]

[a]*Institute for Meteorology and Climate Research – Atmospheric Aerosol Research, Karlsruhe Institute of Technology, Karlsruhe, Germany.*
[b]*Atmospheric Science and Global Change Division, Pacific Northwest National Laboratory, Richland, Washington, USA*

*Corresponding Author. E-mail: seong.moon@kit.edu

Citation:
Hiranuma, N. et al. **A Comprehensive Parameterization of Heterogeneous Ice Nucleation of Dust Surrogate: Laboratory study with Hematite Particles and Its Application to Atmospheric Models**, for *Atmospheric Chemistry and Physics*

Table 1. Summary of aerosol measurements and AIDA ice nucleation experiments. All HALO experiments are from *Skrotzki et al*. (2013).

	Aerosol Measurements			**Ice Nucleation Measurements**				
Experiment ID	Hematite Diameter, nm	Total Number Conc., cm^{-3}	Total Surface Conc., $\mu m^2\ cm^{-3}$	Examined T Range, ˚C	Examined RH_{ice} Range, %	Evaluated n_s, m^{-2}	T(Evaluated n_s), ˚C	RH_{ice}(Evaluated n_s), %
HALO05_24	200	115.0	14.4	-76.1 to -81.9	100.6 to 164.8	10^{11}	-78.2	136.4
HALO04_09	500	112.5	26.9	-75.8 to -80.1	100.3 to 149.8	10^{11}	-77.5	128.3
HALO04_05	500	142.2	30.9	-61.8 to -65.5	100.2 to 135.6	10^{11}	-62.6	111.1
HALO05_18	200	161.9	21.8	-60.3 to -65.2	100.1 to 124.5	10^{11}	-60.8	106.0
HALO06_22	200	145.7	19.2	-50.2 to -53.9	100.3 to 123.4	10^{11}	-50.7	106.7
HALO06_21	200	245.0	32.9	-50.3 to -53.8	100.4 to 115.8	10^{11}	-50.5	102.2
INUIT01_26	1000	342.1	749.0	-41.0 to -47.1	100.2 to 103.9	10^{10}	-41.2	102.2
HALO06_20	200	168.7	22.4	-39.8 to -44.4	100.4 to 128.8	10^{10}	-40.7	111.3
HALO06_19	200	283.0	42.9	-39.7 to -44.5	100.2 to 121.6	10^{10}	-40.6	109.2
INUIT04_08	1000	193.0	647.0	-39.3 to -45.4	100.0 to 113.2	10^{10}	-40.4	110.1
INUIT04_10	1000	161.7	546.6	-37.5 to -43.7	100.0 to 124.1	10^{10}	-40.1	123.3
INUIT01_30	1000	414.5	889.7	-34.6 to -42.0	100.2 to 127.1	2.5×10^8	-37.0	122.8

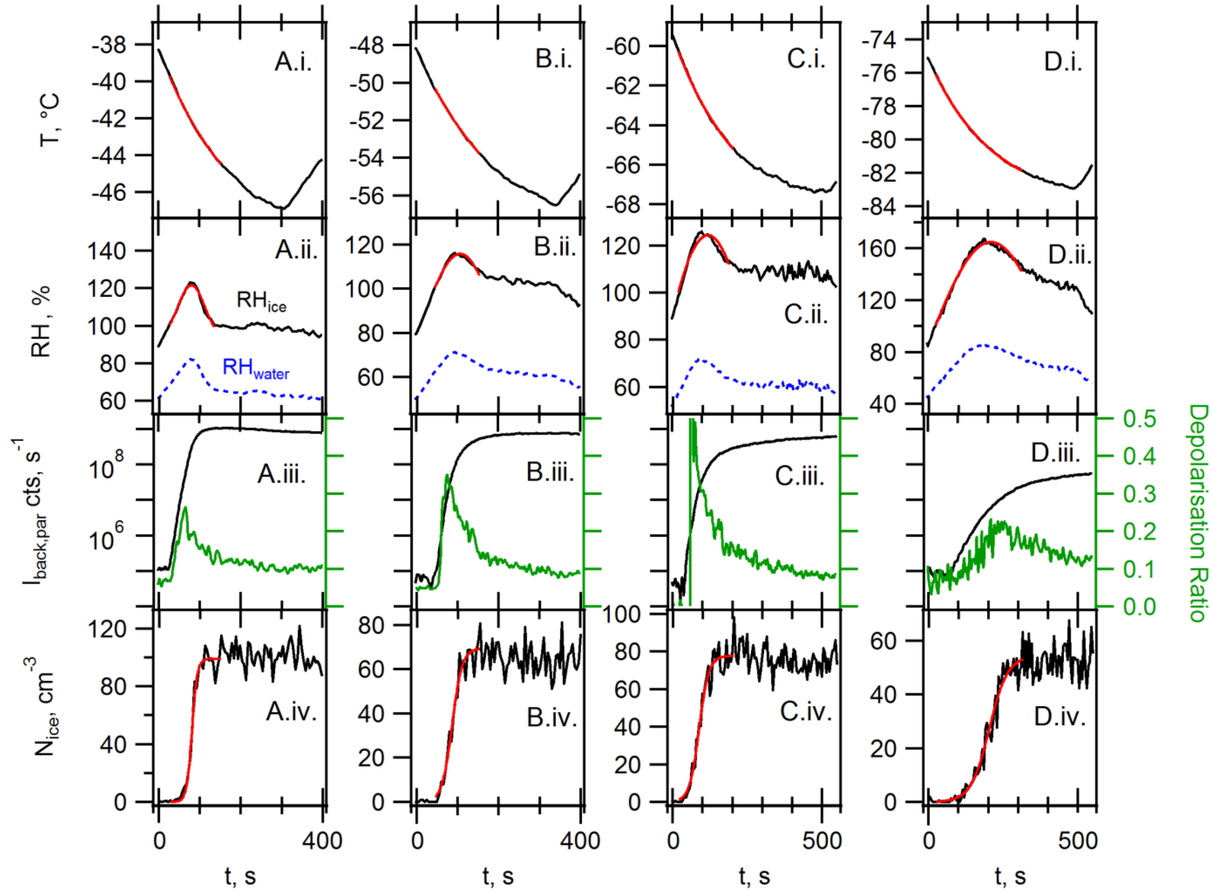

885
886 Figure 1.

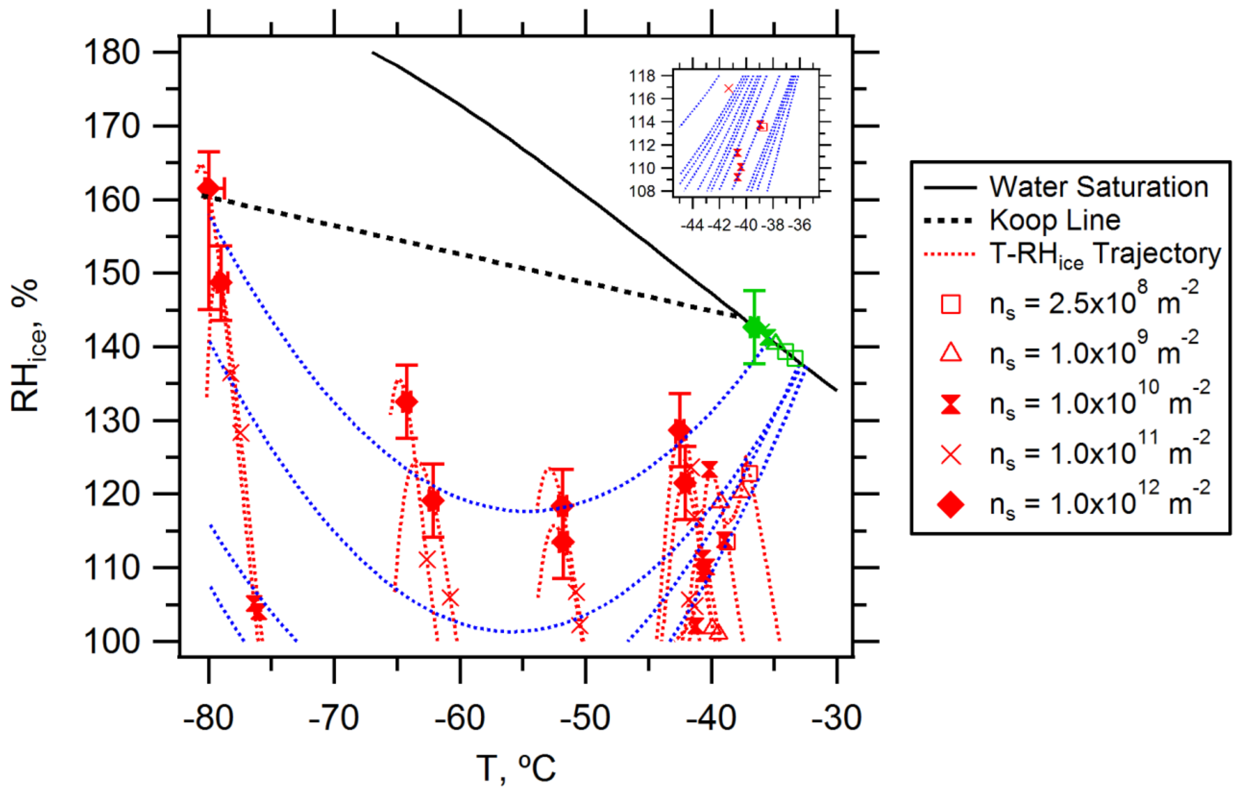

887

888 Figure 2.

889

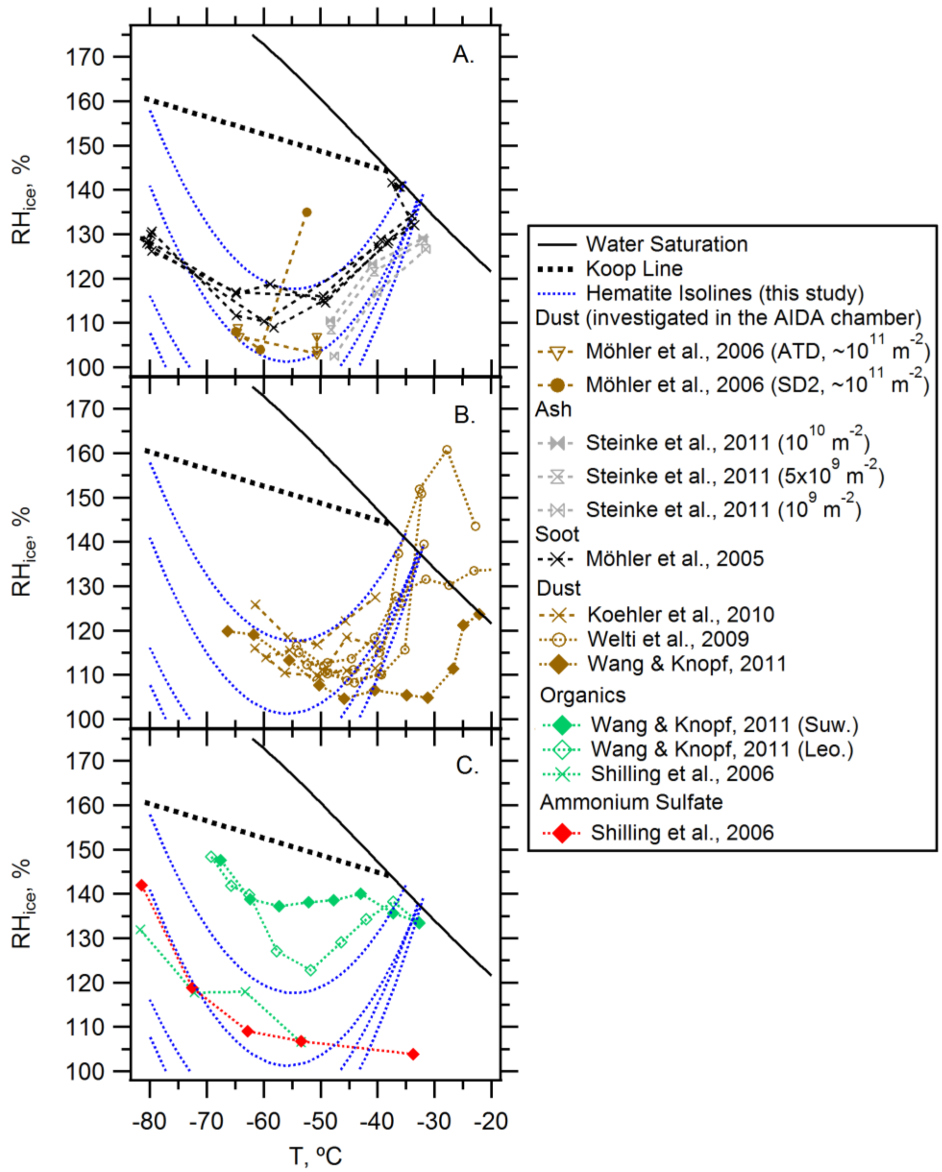

A.
B.
C.
RHice, %
T, ºC
Water Saturation
Koop Line
Hematite Isolines (this study)
Dust (investigated in the AIDA chamber)
Möhler et al., 2006 (ATD, ~10^11 m^-2)
Möhler et al., 2006 (SD2, ~10^11 m^-2)
Ash
Steinke et al., 2011 (10^10 m^-2)
Steinke et al., 2011 (5x10^9 m^-2)
Steinke et al., 2011 (10^9 m^-2)
Soot
Möhler et al., 2005
Dust
Koehler et al., 2010
Welti et al., 2009
Wang & Knopf, 2011
Organics
Wang & Knopf, 2011 (Suw.)
Wang & Knopf, 2011 (Leo.)
Shilling et al., 2006
Ammonium Sulfate
Shilling et al., 2006

Figure 3.

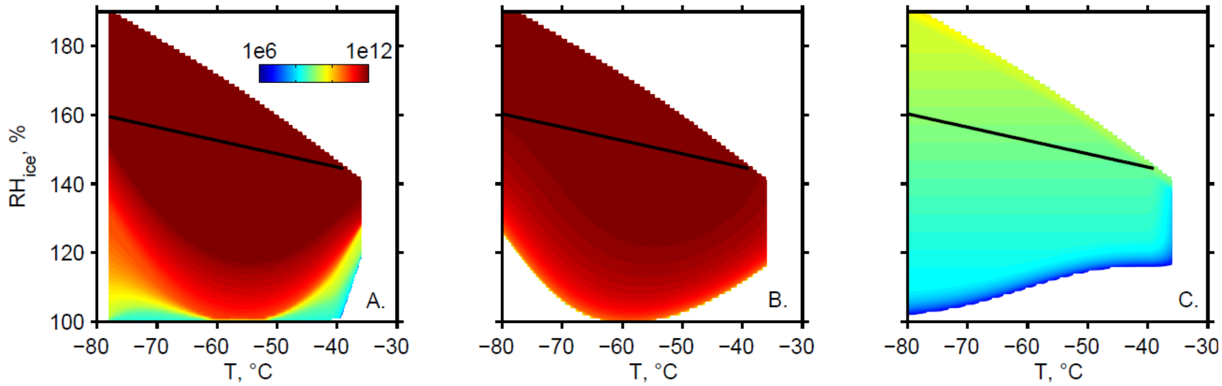

Figure 4.

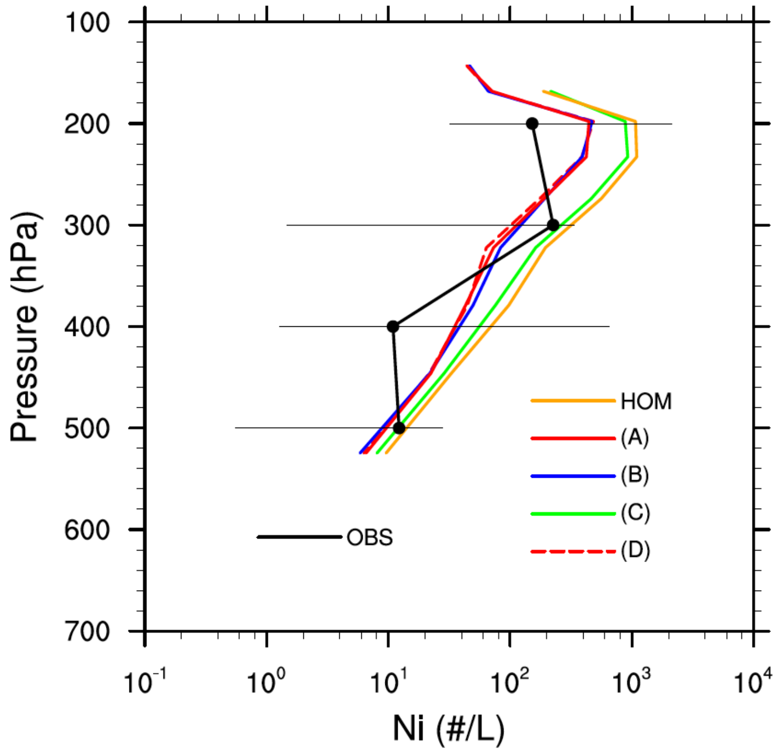
Pressure (hPa)
100
200
300
400
500
600
700
10^{-1}
10^{0}
10^{1}
10^{2}
10^{3}
10^{4}
Ni (#/L)
HOM
(A)
(B)
(C)
(D)
OBS

Figure 5.

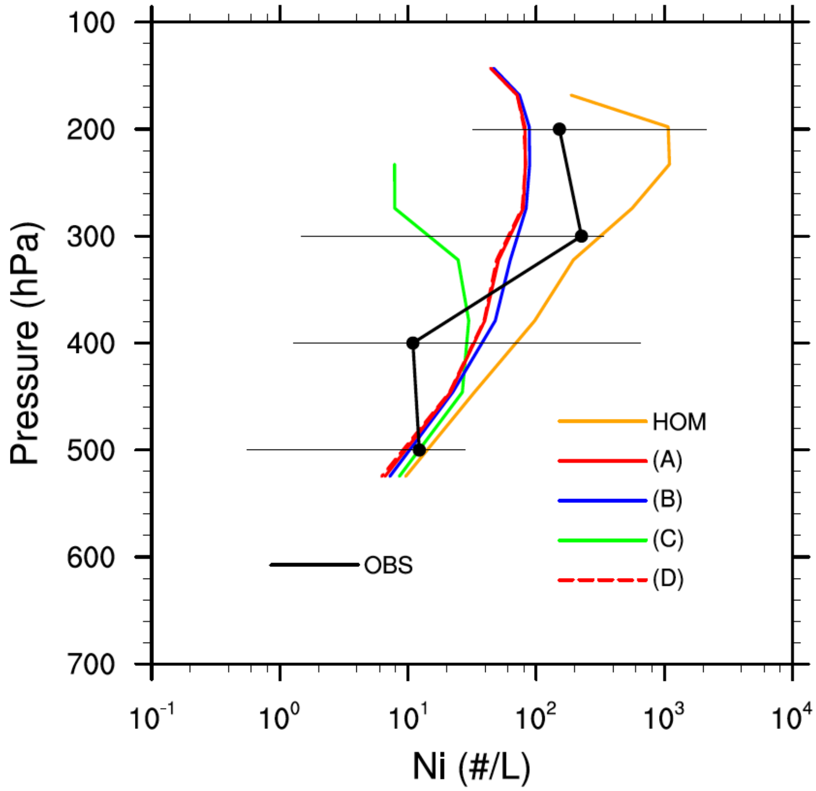
Pressure (hPa)
100
200
300
400
500
600
700
Ni (#/L)
10^{-1}
10^{0}
10^{1}
10^{2}
10^{3}
10^{4}
HOM
(A)
(B)
(C)
(D)
OBS

Figure 6.

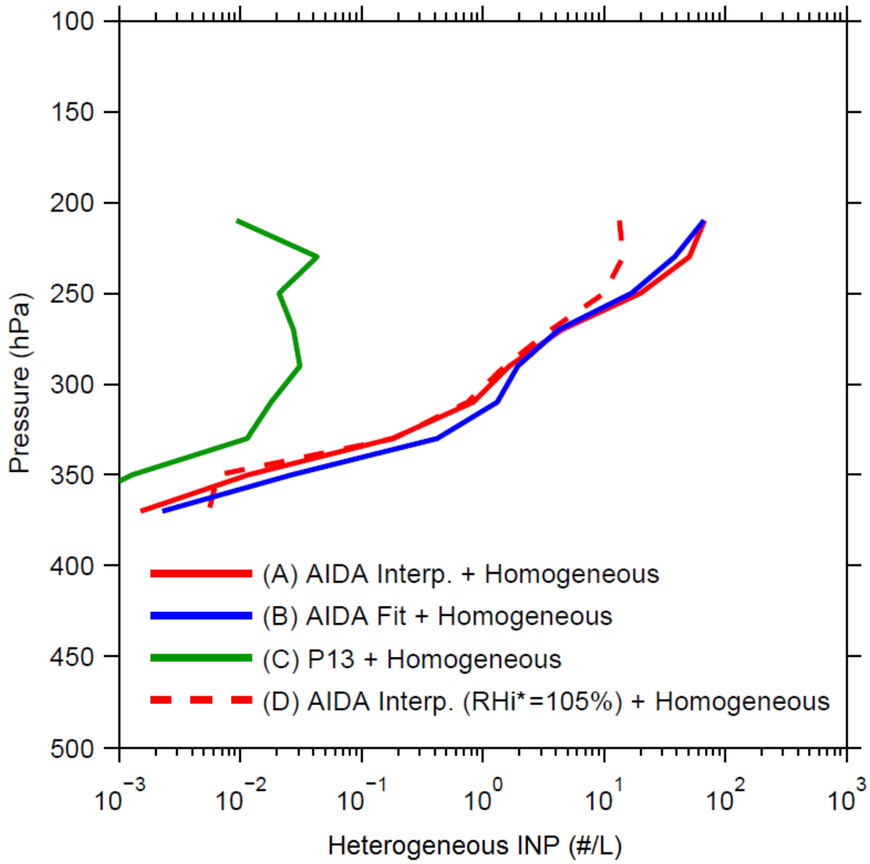

100
150
200
250
300
350
400
450
500
Pressure (hPa)
10^{-3}
10^{-2}
10^{-1}
10^{0}
10^{1}
10^{2}
10^{3}
Heterogeneous INP (#/L)
(A) AIDA Interp. + Homogeneous
(B) AIDA Fit + Homogeneous
(C) P13 + Homogeneous
(D) AIDA Interp. (RHi*=105%) + Homogeneous

Figure 7.

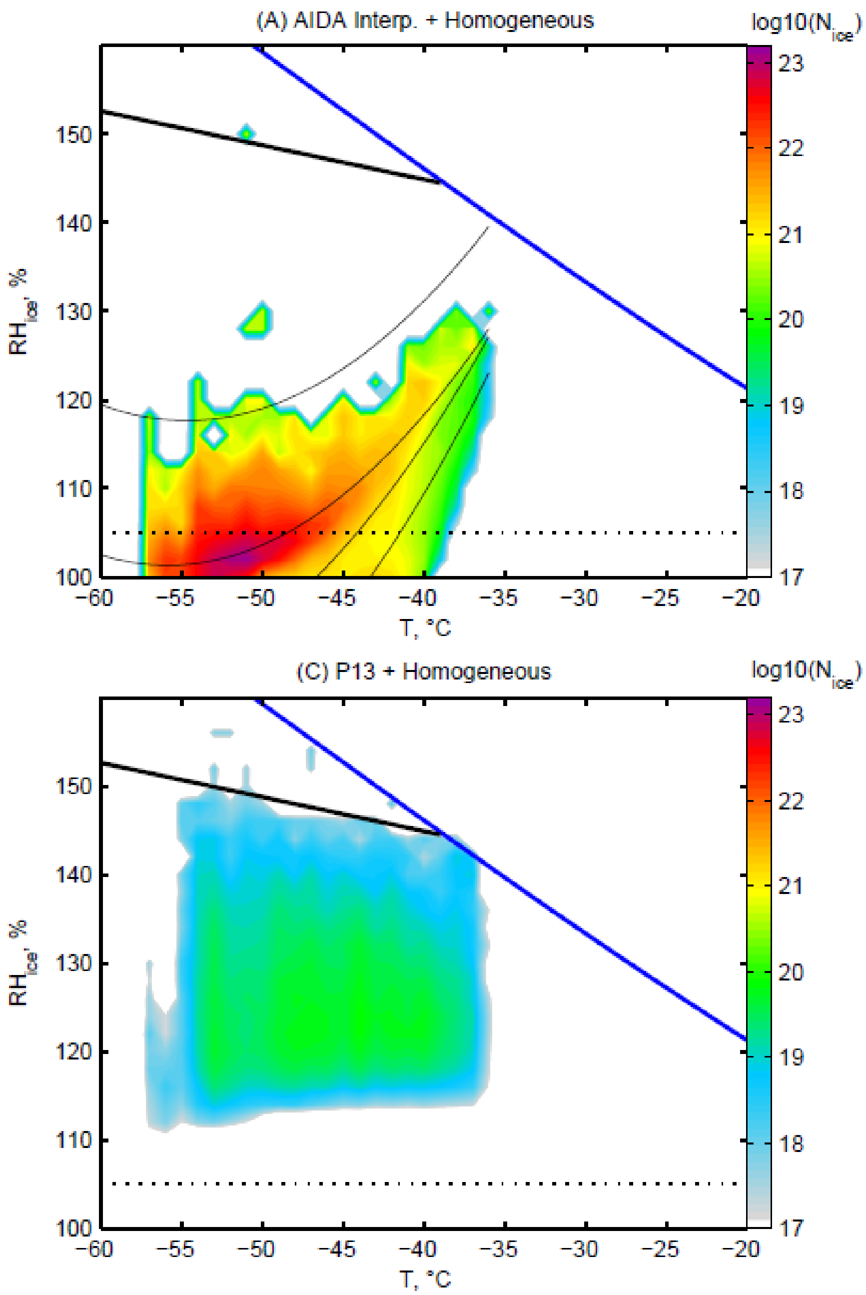
(A) AIDA Interp. + Homogeneous
log10(N_ice)
RH_ice, %
T, °C
23
22
21
20
19
18
17
150
140
130
120
110
100
−60
−55
−50
−45
−40
−35
−30
−25
−20
(C) P13 + Homogeneous
log10(N_ice)
RH_ice, %
T, °C

Figure 8.

Figure Captions

Figure 1. Temporal plots of the representative AIDA deposition mode freezing experiments with various cooling ranges, including A. HALO06_19, B. HALO06_21, C. HALO05_18 and D. HALO05_24. Panels are arranged to show the measurements of i. AIDA mean gas temperature (*T*), ii. TDL, iii. SIMONE and iv. ice crystal concentration (N_{ice}). Note that the red lines represent interpolated data used for the n_s-isoline formulation. The $I_{back,par}$ in Panel iv axis denotes the backscattered light scattering intensity parallel to the incident polarisation state (log-scaled). An increase in the depolarisation ratio indicates the formation and growth of ice crystals.

Figure 2. The constant n_s magnitudes are joined by lines (blue), representing "isolines" of hematite freezing profiles in the T-RH_{ice} space. The interpolated isolines are equally spaced at every order of magnitude from 10^{12} m^{-2} (top) to 10^{9} m^{-2} (bottom). Experimental trajectories of AIDA expansion-experiments with hematite particles are shown as red dotted lines. The data indicated by green color on the water saturation line represent the previously reported results of immersion freezing (*Hiranuma et al*., 2014). The sub-panel shows a magnified section of *T* (-35 ºC to -45 ºC) and RH_{ice} (110 to 120 %) space with equi-distant n_s spacing (every quarter magnitude). The error bars at n_s of 10^{12} m^{-2} are from welas.

Figure 3. Ice nucleation onset T-RH_{ice} of previously published data (A. AIDA studies, B. dust, and C. ammonium sulfate and organics) shown together with the isolines of hematite particles from the present study (10^{12} m^{-2}, top, to 10^{9} m^{-2}, bottom).

Figure 4. Spatial plot of isolines for constant n_s derived from A. interpolating AIDA data, B. applying the third degree polynomial fit function to interpolated AIDA data and C. a previously published parameterization (*Phillips et al*., 2013) for hematite particles. The color scale displays log-scaled n_s values in m^{-2}, applicable to all panels. The solid black lines indicate the homogeneous freezing threshold line (i.e., Koop line).

Figure 5. Monthly mean profiles of the simulated in-cloud ice crystal number concentrations (*Ni* ~ N_{ice}) over the ARM SGP site. The four cases shown in the figure include the pure

homogeneous ice nucleation case (HOM) and four combined (heterogeneous + homogeneous) ice nucleation cases: (A) AIDA Interp. + Homogeneous; (B) AIDA Fit + Homogeneous; (C) P13 + Homogeneous; and (D) AIDA Interp. (RH_i^*=105%) + Homogeneous. Black dots show the observed mean profile of *Ni*. Left and right ends of the horizontal bars indicate the 10^{th} and 90^{th} percentiles of the observed *Ni* values at each pressure level.

Figure 6. Monthly mean profiles of the simulated in-cloud ice crystal number concentrations (*Ni* ~ N_{ice}) over the ARM SGP site. The four cases shown in the figure include the pure homogeneous ice nucleation case (HOM) and four pure heterogeneous ice nucleation cases: (A) AIDA Interp.; (B) AIDA Fit; (C) P13; and (D) AIDA Interp. (RH_i^*=105%). Black dots show the observed mean profile of *Ni*. Left and right ends of the horizontal bars indicate the 10^{th} and 90^{th} percentiles of the observed *Ni* values at each pressure level.

Figure 7. The mean heterogeneous INP number concentrations (~N_{ice}) simulated in COSMO. The red dashed line represents the simulation with 105% RH_{ice} as the lower boundary of ice formation, while the others are based on with 100% for the minimum RH_{ice} value.

Figure 8. Accumulated ice crystal concentrations (color scale in total crystals per model domain) as a function of temperature (1˚C bins) and RH_{ice} (2% bins). Heterogeneous nucleation simulated by AIDA parameterization (i.e., Figure 4A) and P13 parameterization (i.e., Figure 4C) was combined with homogeneous nucleation of cloud droplets.